npj | climate and atmospheric science

Article

Published in partnership with CECCR at King Abdulaziz University

https://doi.org/10.1038/s41612-024-00594-5

Winter precipitation predictability in Central Southwest Asia and its representation in seasonal forecast systems

Matthew F. Horan [1,2,3] ✉, Fred Kucharski[4], Nathaniel Johnson [5] & Moetasim Ashfaq [1]

In Central Southwest Asia (CSWA; 22°N to 40°N and 30°E to 70°E), winter (November to February) precipitation contributes up to 70% of the annual mean, but substantial interannual variations exist. Dynamical models exhibit subpar predictability in this region, but the limits of their skills are not well established. Here, we identify the tropical and extratropical forcings that explain ~75% of area-averaged seasonal variability in CSWA winter precipitation. Tropical forcing comes from the indirect El Niño-Southern Oscillation (ENSO) pathway, the leading mode of tropical Indian Ocean precipitation variability. This mode is coupled with ENSO-related Pacific Ocean sea surface temperature variability. A direct ENSO influence on CSWA does not extend beyond its Indian Ocean connection. Extratropical forcing comes from a large-scale mode of internal atmospheric variability. The spatial structure, variability of tropical forcing, and teleconnection with CSWA winter precipitation are skillfully depicted in two seasonal forecasting systems: the fifth-generation seasonal forecasting system (SEAS5) and Seamless System for Prediction and Earth System Research (SPEAR). Extratropical forcing's spatial structure is also produced skillfully in the two modelling systems; however, the representation of its interannual variability and teleconnection requires improvement. While SEAS5 displays skill in representing extratropical forcing influence on CSWA winter precipitation and marginal skill in reproducing interannual variability, SPEAR has negligible ability in both areas. Consequently, these models have limited predictive skills over CSWA in winter. While improvements in representing extratropical forcing may be inherently limited as it arises from internal atmospheric variability, further research is needed to establish its predictability limits fully.

The Central and Southwest Asia (CSWA) region includes countries or parts of countries in South, West, and Central Asia with arid to semi-arid climates. Many countries within the CSWA are drought-prone and water-stressed[1–4], as precipitation exhibits strong seasonality and substantial year-to-year variability[5–7]. Most of the region except parts of the western Himalayas receives the predominant fraction (up to 90%) of annual precipitation during winter and spring (November to April; Supplementary Fig. 1), known as the wet season. Extratropical weather systems or *western disturbances* are the most effective synoptic-scale precipitation-producing mechanisms that facilitate moisture transport from oceanic and terrestrial evaporative sources during the wet season in this region[8,9]. A subtropical westerly jet that spans northern Africa to East Asia facilitates the movement of weather systems through the CSWA, and changes in its characteristics influence precipitation distribution[5,6,10–12].

Because of precipitation seasonality in CSWA and the high vulnerability of the region's population to natural and forced climate

[1]Computational Sciences and Engineering Division, Oak Ridge National Laboratory, Oak Ridge, TN, USA. [2]Bredesen Center, University of Tennessee, Knoxville, TN, USA. [3]Department of Engineering Physics, Air Force Institute of Technology, Wright-Patterson Air Force Base, Dayton, OH, USA. [4]Earth System Physics, Abdus Salam International Centre for Theoretical Physics, Trieste, Italy. [5]National Oceanic and Atmospheric Administration/Geophysical Fluid Dynamics Laboratory, Princeton, NJ, USA. ✉e-mail: matthew.horan.1@au.af.edu

variations[7,9,12–16], significant scientific efforts have been carried out over the past decades to understand the drivers of wet season precipitation variability and change. Natural modes of variability influencing precipitation distribution in the region have been identified primarily by examining connections between sea surface temperature (SST) variability in the tropical Pacific, the El Niño-Southern Oscillation (ENSO), and the most prevalent atmospheric variability pattern in the northern hemisphere, the North Atlantic Oscillation (NAO). For most of the 21st century, studies have suggested that both natural modes of variability have a positive teleconnection with wet season precipitation in CSWA[3,7,14,17]. However, recent studies demonstrate a lack of spatial robustness and sub-seasonal consistency in their influences[9,18–20].

According to Abid et al.[18], ENSO influences CSWA precipitation through two pathways. The direct pathway is via an eastward propagating Rossby wave originating in the central Pacific. This influence lacks persistence at the sub-seasonal scale and varies between positive to no influence. The indirect pathway is via ENSO-induced precipitation anomalies in the tropical Indian Ocean, which generate a Rossby wave response in the higher latitudes. This indirect influence is also positive and persists throughout the season when analyzed on a monthly timescale. Mehmood et al.[9] further establish that the tropical Indian Ocean's influence via atmospheric diabatic heating anomalies is among the strongest remote teleconnections over the CSWA region at a monthly timescale. The authors also note that the NAO's influence on CSWA precipitation is inconsistent sub-seasonally and not among the strongest. Instead, other modes representing the northern hemisphere's internal atmospheric variability, such as the East Atlantic Mode (EAM) and East Atlantic West Russia pattern (EAWR), are more substantial and sub-seasonally consistent contributors to precipitation variability over CSWA. EAWR's role in precipitation variability has also been established by Rana et al.[15] Mehmood et al.[9] also highlights the importance of tropical-extratropical interactions in the propagation of tropical forcing over CSWA.

The understanding that tropical and extratropical modes of variability contribute to year-to-year variations in precipitation over the CSWA motivates investigation of how predictable these modes are at a seasonal scale and how well their teleconnections are represented in state-of-the-art seasonal forecasting systems. The accuracy or inaccuracy of models in representing the interannual variability of these natural forcings and describing their teleconnections with CSWA precipitation may provide insight into the causes of seasonal prediction capabilities or shortcomings over this region. Earlier studies focusing on sub-regions within CSWA suggested a limited skill in predicting wet season precipitation[14,21–27]. Seasonal forecasting systems are less confident in predicting interannual variability of extratropical forcings than tropical forcings[28–30] though some promise has been noted in predicting NAO[31] and EAM[30]. The extent to which their lack of skill regarding CSWA wet season precipitation is caused by their inherent limitations in representing extratropical climate variability remains to be determined. Moreover, since previous investigations regarding the potential predictability of precipitation over CSWA, the Geophysical Fluid Dynamics Laboratory (GFDL) and the European Center for Medium-Range Weather Forecasts (ECMWF) have developed new next-generation seasonal prediction modelling systems[32,33], Seamless System for Prediction and Earth System Research (SPEAR), and the fifth-generation seasonal forecasting system (SEAS5).

These updated modelling systems still need to be evaluated over CSWA for their effectiveness.

Using recent advancements in understanding CSWA winter precipitation variability and new seasonal prediction modelling systems, this study aims to achieve two goals. The first goal is to develop a seasonal-scale statistical model representing year-to-year CSWA precipitation variability after minimizing the number of independent variables selected from the natural modes of variability. We only focus on the winter months (November to February) due to the inhomogeneity of dynamic and thermodynamic processes regulating precipitation-generating mechanisms in winter and spring[9]. The second objective is to examine how the SPEAR and SEAS5 seasonal prediction modelling systems represent the identified sources of predictability of CSWA winter precipitation and how the representation of these independent forcings affects their skillfulness over the region.

Results and discussion

Dominant ENSO forcing

We use Empirical Orthogonal Function (EOF) analysis to examine SST variability in the equatorial Pacific Ocean and precipitation variability in the tropical Indian Ocean (see "Methods" section). In the Pacific Ocean between 10°S to 10°N and 160°W to 80°E, the first EOF of winter SST explains 83% (81%) of the variance in ERA5 (MERRA2) (Fig. 1a, Supplementary Fig. 2). It exhibits a zonal maximum in the equatorial region and represents ENSO-related SST variability. There is a high correlation between the associated Principal Component of the first EOF (PC1) and all four Niño indexes (Fig. 1b, Supplementary Fig. 2). For this study, we preferred the EOF-based ENSO index over the Niño indexes since it represents SST variability in the entire equatorial Pacific region and helps address ENSO diversity influencing its teleconnections. In the tropical Indian Ocean between 10°S to 10°N and 40°E to 140°E, the first EOF of precipitation accounts for 38% (36%) of the variance in ERA5 (MERRA2). There is a semi-zonal dipole pattern with stronger (weaker) precipitation in the western (eastern) tropical Indian Ocean. A tongue of wet anomalies extends eastward into the equatorial Indian Ocean from the western Indian Ocean. The associated PC1 time series highly correlates with the index defined by Abid et al.[18] using precipitation differences over the western and Indian Ocean regions (Fig. 1c). The EOF-based precipitation index is preferred for this study as it is less sensitive to the selection of boxes for defining the precipitation dipole in the western and eastern Indian Oceans. We refer to the EOF-based precipitation dipole in the tropical Indian Ocean as the Indian Ocean Precipitation Dipole (IOPD) in the rest of the manuscript.

A high correlation (ERA5: 0.86, MERRA2: 0.87) exists between IOPD and ENSO on a seasonal scale. As previously noted, earlier studies described IOPD as indirect ENSO forcing, resulting from anomalies in the Indian Ocean's Walker circulation branch. The ENSO-induced atmospheric anomalies in the Walker circulation cause a precipitation anomaly dipole in the tropical Indian Ocean with above- (below-) average precipitation in the western (eastern) Indian Ocean during the positive ENSO phase and vice versa. The precipitation response to ENSO forcing leads to a diabatic heating dipole in the atmosphere above the tropical Indian Ocean. A numerical model experiment incorporating such diabatic anomalies produces Rossby wave propagation in higher latitudes, influencing the precipitation distribution remotely over distant regions[18].

The seasonal-scale correlation between IOPD and ENSO, shown in this study, is far more robust than the monthly correlation reported in earlier studies[9,18,34]. The high correlation suggests that both direct and indirect forcings may not be necessary to explain ENSO's seasonal-scale influence on CSWA precipitation variability. We investigate this possibility in several ways. First, we calculate the Pearson correlation between the CSWA precipitation index and tropical forcings (ENSO, IOPD) by analyzing their interannual anomalies. Second, we perform the regression of CSWA precipitation anomalies onto ENSO and IOPD indexes to understand their remote influences' strength, direction, and spatial characteristics. Lastly, we perform partial correlation analyses to examine the association of ENSO forcing with CSWA precipitation while controlling for the IOPD effect and vice versa.

We would like to briefly describe CSWA winter precipitation characteristics before presenting the results of these analyses. The climatological precipitation distribution over most high-elevation regions in CSWA is about 5 millimetres day^{-1} during winter (Fig. 2a, Supplementary Figs. 3–5). These include the western Himalayas and Karakoram in Pakistan, the Pamir Mountains in Tajikistan, and the Zagros Mountains in Iran. Other mountain ranges with relatively high magnitudes of winter precipitation include the Hindukush in Pakistan and Afghanistan. Winter precipitation in the rest of the CSWA region ranges from less than 1 mm day^{-1} to ~2 mm day^{-1}. The

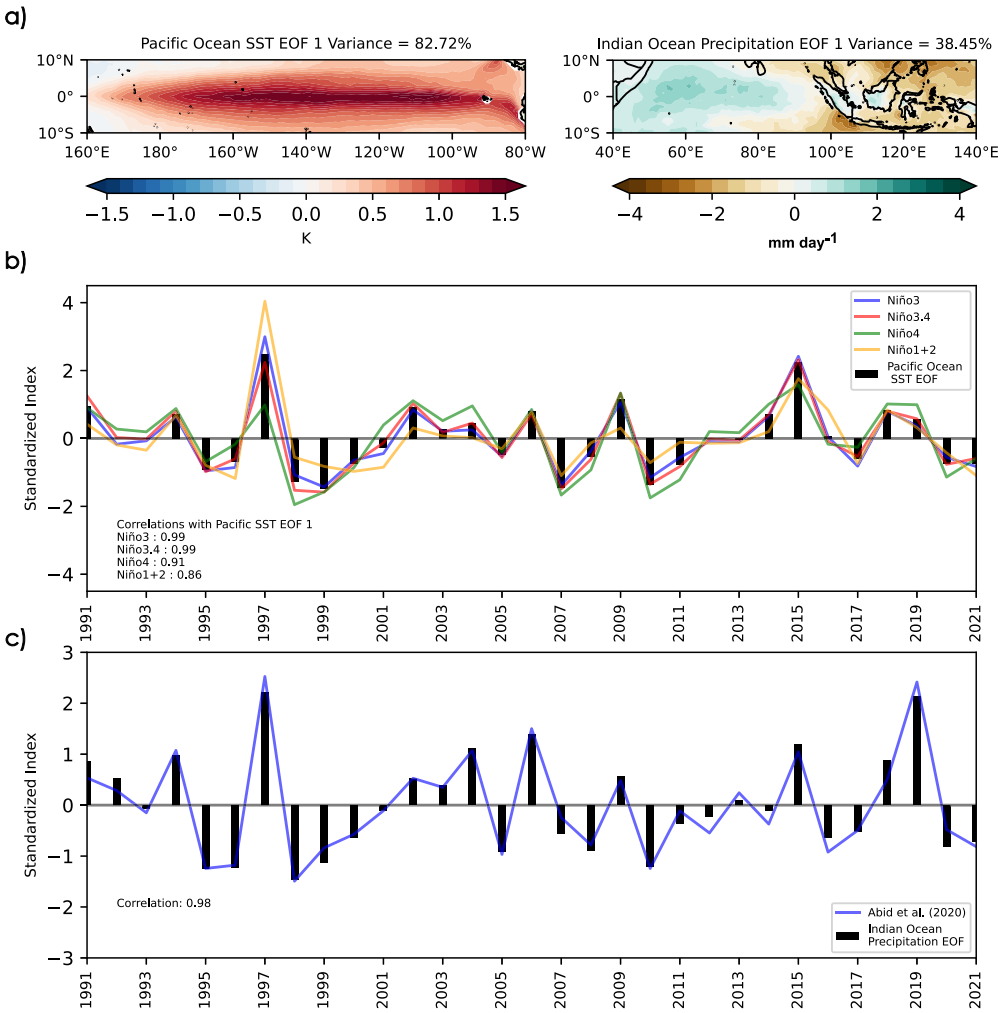

Fig. 1 | Tropical forcing indexes. a The first EOF patterns (EOF1) of the 1991–2022 winter (November to February) related to the Pacific Ocean SST (K) and the Indian Ocean precipitation (mm day^{-1}). **b** Standardized Nino indexes and PC time series of Pacific Ocean SSTs EOF1. **c** Standardized precipitation-based index based on Abid et al. (2020) and PC time series of Indian Ocean precipitation EOF1. The results are based on ERA5 reanalysis.

spatial distribution of interannual winter precipitation variability is generally proportional to seasonal averages (Fig. 2a and Supplementary Figs. 3–5).

The CSWA precipitation index is well correlated with ENSO and IOPD indexes at the seasonal level. It has a 0.62 (0.6) correlation with ENSO and a 0.7 (0.69) correlation with IOPD in ERA5 (MERRA2) (Fig. 2b, Supplementary Fig. 4). The spatial patterns based on the regression of CSWA precipitation onto ENSO and IOPD indexes reveal a predominantly positive influence of similar characteristics throughout the region. Both regressions show statistically significant teleconnections over a broad zonal area between the northern Arabian Peninsula (Iraq, Syria) and northern Pakistan. Regression coefficients are more robust over mountain ranges in Pakistan, Afghanistan, Tajikistan, and Iran, which receive relatively higher winter precipitation (Fig. 2c and Supplementary Fig. 4). ENSO and IOPD also exert a significant favourable influence over the central Arabian Peninsula. In addition to these positive influences common to both forcings, the IOPD also exerts substantial positive effects on southern Iran and central and west Pakistan. This influence is nonexistent in ENSO's teleconnection. Partial correlation analyses further explain the dominance of IOPD (indirect ENSO) forcing over direct ENSO forcing in the case of CSWA winter precipitation. While controlling for the ENSO effect, the linear relationship between IOPD and CSWA precipitation remains statistically significant in several parts of Pakistan, Afghanistan, and Iran. The most notable exception is Tajikistan, where IOPD's significant positive influence becomes insignificantly negative after controlling for ENSO's effect (Fig. 2d, Supplementary Fig. 4). When averaged over CSWA, the IOPD partial correlation is 0.42 (0.41) in ERA5 (MERRA2).

Conversely, most ENSO teleconnection in the region becomes insignificant positive or reverses to weak negative, leading to 0.05 (0.01) area-averaged partial correlation in ERA5 (MERRA2). When taken together, Pearson correlation, linear regression, and partial correlation analyses suggest that the IOPD alone can best describe ENSO's seasonal-scale teleconnection with CSWA precipitation and that including direct ENSO forcing may not uniquely account for its remote influence further. This point is additionally supported by the multilinear regression analysis described later.

Extratropical forcings

Previous studies have highlighted the importance of extratropical forcings in shaping precipitation variability in the CSWA region[4,7,14,15,25,35]. Various modes of atmospheric variability in the northern hemisphere have been identified as extratropical forcings, including the NAO, EAM, and EAWR. The Climate Prediction Center (CPC) at National Oceanic and Atmospheric Administration (NOAA) uses rotated EOF analyses on monthly 200-hPa geopotential height to distinguish these modes sub-seasonally[36]. Consequently, the CPC-defined monthly indexes of these modes are, by definition, uncorrelated. However, when averaged seasonally, these modes can coexist and correlate, so it is not straightforward to identify their independent teleconnections with CSWA precipitation. Moreover, tropical

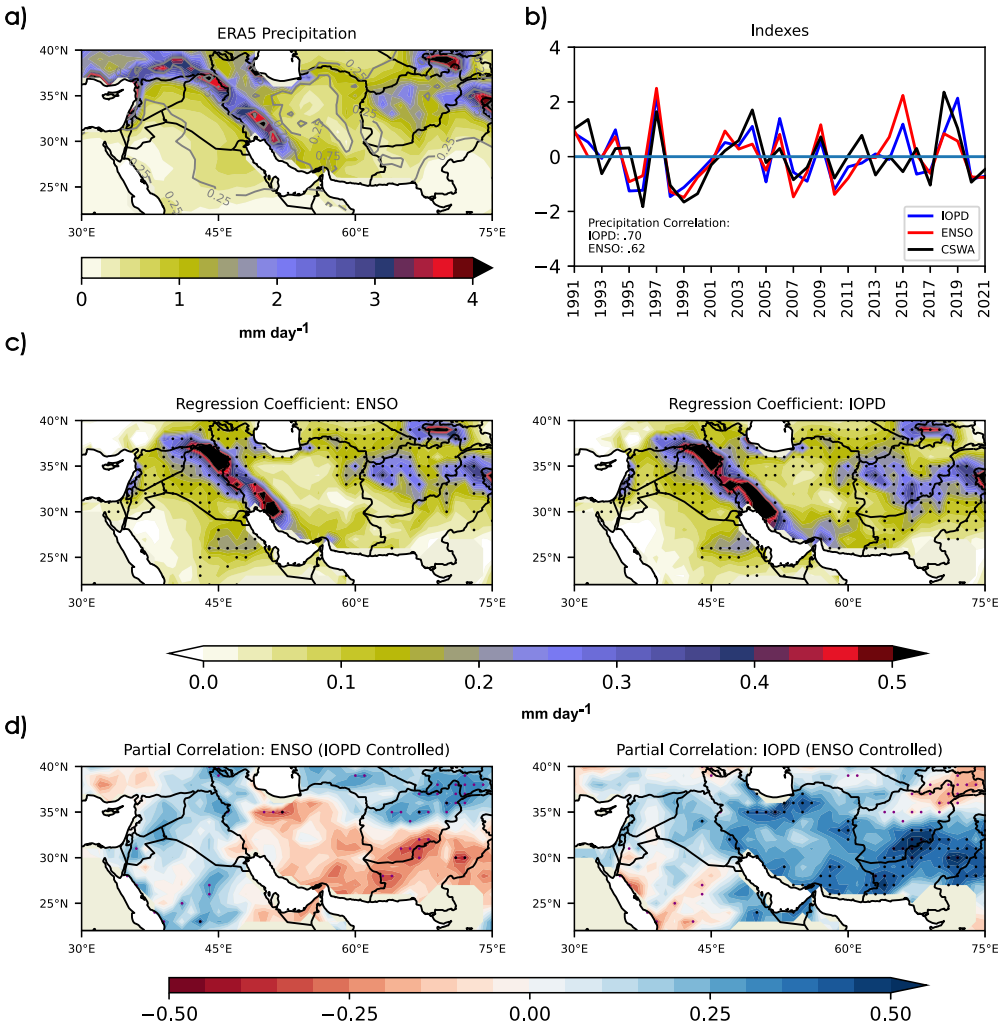

Fig. 2 | CSWA precipitation and tropical teleconnections. a Average precipitation (color; mm day^{-1}) and standard deviation (contour; mm day^{-1}). **b** Standardized time series of CSWA precipitation, ENSO, and IOPD. **c** Regression of CSWA precipitation (mm day^{-1}) onto standardized ENSO and IOPD Indices. **d** Partial correlation of ENSO and IOPD with CSWA precipitation. Stippling indicates significance at the 95% confidence level.

forcings, such as ENSO and IOPD, can also project onto these modes to remotely influence distant regions[9,37,38].

Therefore, to identify the most relevant seasonal-scale atmospheric variability pattern related to the CSWA precipitation, we perform EOF analyses on 200-hPa geopotential height anomalies over a region between 20°W to 150°E and 20°N to 70°N after linearly removing the influence of ENSO and IOPD from geopotential height. The first three EOFs (Supplementary Fig. 4) pass the North's uniqueness test and explain ~60% of the residual variance in ERA5 and MERRA2. However, only the second EOF (EOF2) is significantly related to CSWA winter precipitation variability, which represents 19.3% (18.5%) of variance in ERA5 (MERRA2). The PC time series associated with EOF2 (PC2) displays a 0.51 (0.5) correlation with the CSWA precipitation index in ERA5 (MERRA2). The corresponding correlation of PC2 with the residual CSWA precipitation index after removing IOPD influence is 0.71 (0.69).

The spatial pattern in EOF2 consists of a high over the eastern Atlantic Ocean/western Europe and a zonally elongated trough at the subtropical latitudes spanning the CSWA region. The pattern also exhibits a relatively weak high over Mongolia and Siberia. This atmospheric pattern closely resembles several named Northern Hemisphere atmospheric modes. This point is explained by regressing the geopotential height anomalies onto the CPC indexes after linearly removing tropical forcings from both, then calculating the correlation between EOF2 and the regressed patterns. The most prominent is the negative EAM pattern, which exhibits a pattern correlation of 0.85 (0.88) in ERA5 (MERRA2) (Fig. 3b, Supplementary Figs. 7, 8). A high temporal correlation exists between the EAM index and PC2 (ERA5: −0.59, MERRA2: −0.58). A significant association has also been found between EOF2 and EAWR and polar Eurasian (POL/EUR) patterns. The pattern correlation between EOF2 and EAWR (POL/EUR) is 0.74 and 0.76 (0.79 and 0.75) in ERA5 and MERRA2, respectively (Supplementary Figs. 5, 6). The temporal correlation between the EAWR index and PC2 is 0.43 (0.5) in ERA5 (MERRA2), while that between POL/EUR and PC2 is 0.44 (0.43). These comparisons suggest that the EOF2 of the 200-hPa geopotential height predominantly represents those modes of atmospheric variability in the northern hemisphere that shape interannual precipitation variability over CSWA in winter. After linearly removing tropical forcing from their indexes, EAM, EAWR, POL/EUR also exhibit significant but weaker than IOPD correlation with the CSWA precipitation index in ERA5 (EAM = −0.47; EAWR = 0.30; POL/EUR = 0.41) and MERRA2 (EAM = −0.44; EAWR = 0.39; POL/EUR = 0.42).

The influence of some of these extratropical forcings on CSWA precipitation at seasonal and sub-seasonal scales has also been reported in earlier studies[9,15]. For example, Mehmood et al.[9] found that the EAM had the most substantial negative impact on monthly CSWA winter precipitation. Additionally, Mehmood et al.[9] and Rana et al.[15] demonstrated a positive influence of EAWR on a monthly and seasonal basis. Therefore, we assume that a multilinear regression model representing tropical (IOPD) and extratropical forcing (PC2 of 200-hPa geopotential height)

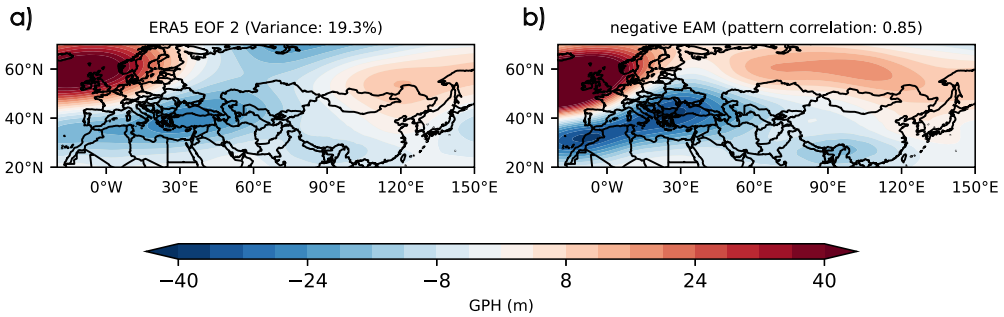

Fig. 3 | CSWA-relevant extratropical forcing. a The second EOF of 200-hPa geopotential height after linearly removing ENSO and IOPD influences. **b** The regression of 200-hPa geopotential height onto the negative East Atlantic Mode.

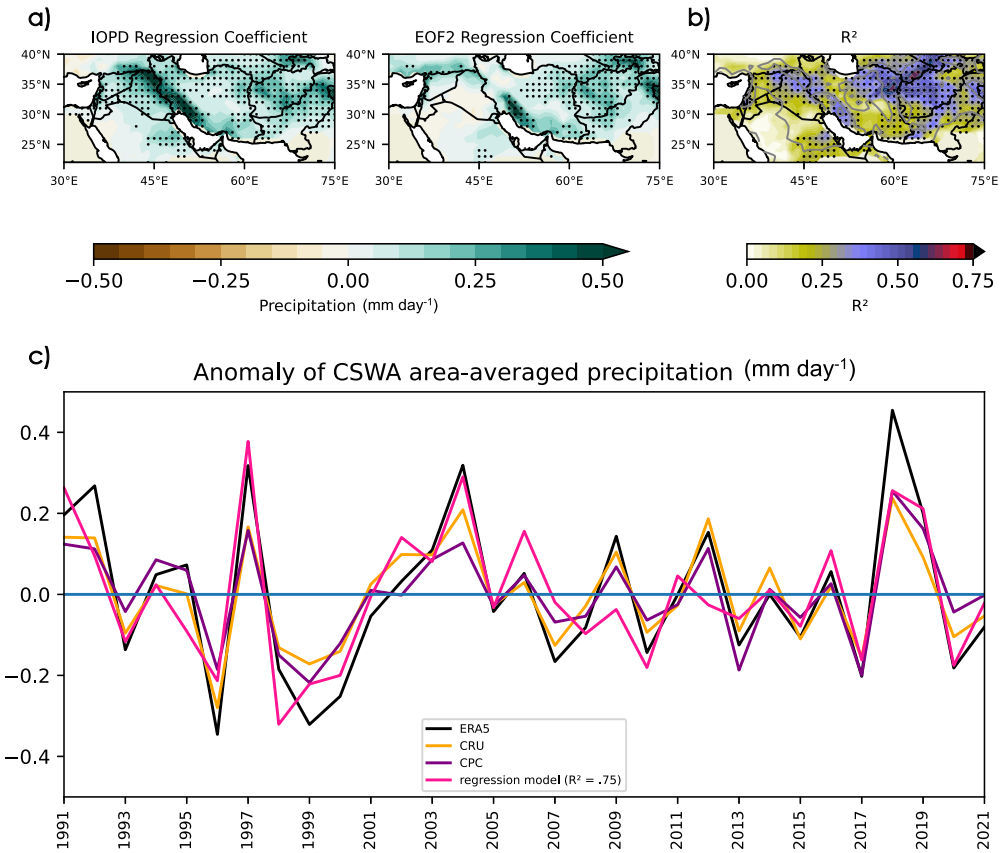

Fig. 4 | Multilinear regression analyses. a Partial regression coefficients of IOPD and PC2. Stippling indicates significance at the 95% confidence level. **b** the coefficient of determination (r-squared) based on the multilinear model. Stippling indicates the statistical significance of the *F*-test ($p < 0.05$). **c** Area-averaged precipitation time series in ERA5, CRU, CPC, and regression model. The results are based on ERA5 reanalysis and r-squared values are available in the legend.

forcings should explain a substantial part of CSWA precipitation variability in winter.

Multilinear regression analysis

We construct a multilinear regression model using IOPD (tropical) and PC2 of 200-hPa geopotential height (extratropical) as independent forcings and CSWA precipitation as a dependent variable. Given that IOPD and PC2 are independent, the partial regression coefficient describing IOPD influence (Fig. 4, Supplementary Fig. 8) is similar to that shown in Fig. 2b. Extratropical forcing influence is significantly positive over northern and southwest Pakistan, Tajikistan, Afghanistan, and parts of Iran. Limited extratropical influence is also present in parts of the Arabian Peninsula, consistent with earlier studies[3,8,39,40]. In addition to regression coefficients, we also provide the correlation between precipitation and the two forcings over CSWA (Supplementary Fig. 10), which shows a predominantly positive influence of extratropical forcing across CSWA except in the northern Arabian Peninsula, where it is insignificantly negative. Spatially, the combined effect of tropical and extratropical forcings explains up to 75% of precipitation variance over CSWA in winter, with the strongest magnitude of the coefficient of determination (r-squared) over northeast Iran, southern Turkmenistan, and Afghanistan (Fig. 4, Supplementary Fig. 9). The r-squared values in southeastern Pakistan, central Iran, and the western Arabian Peninsula are negligible due to low precipitation magnitudes and variability.

The regression model accurately represents most of the interannual variability of spatially averaged CSWA winter precipitation. This is particularly true in exceptionally dry (1996, 1998, 2017) and wet (1997, 2004, 2018) years. The spatially averaged precipitation using the regression model represents 75% (72%) of ERA5 (MERRA2) precipitation variability.

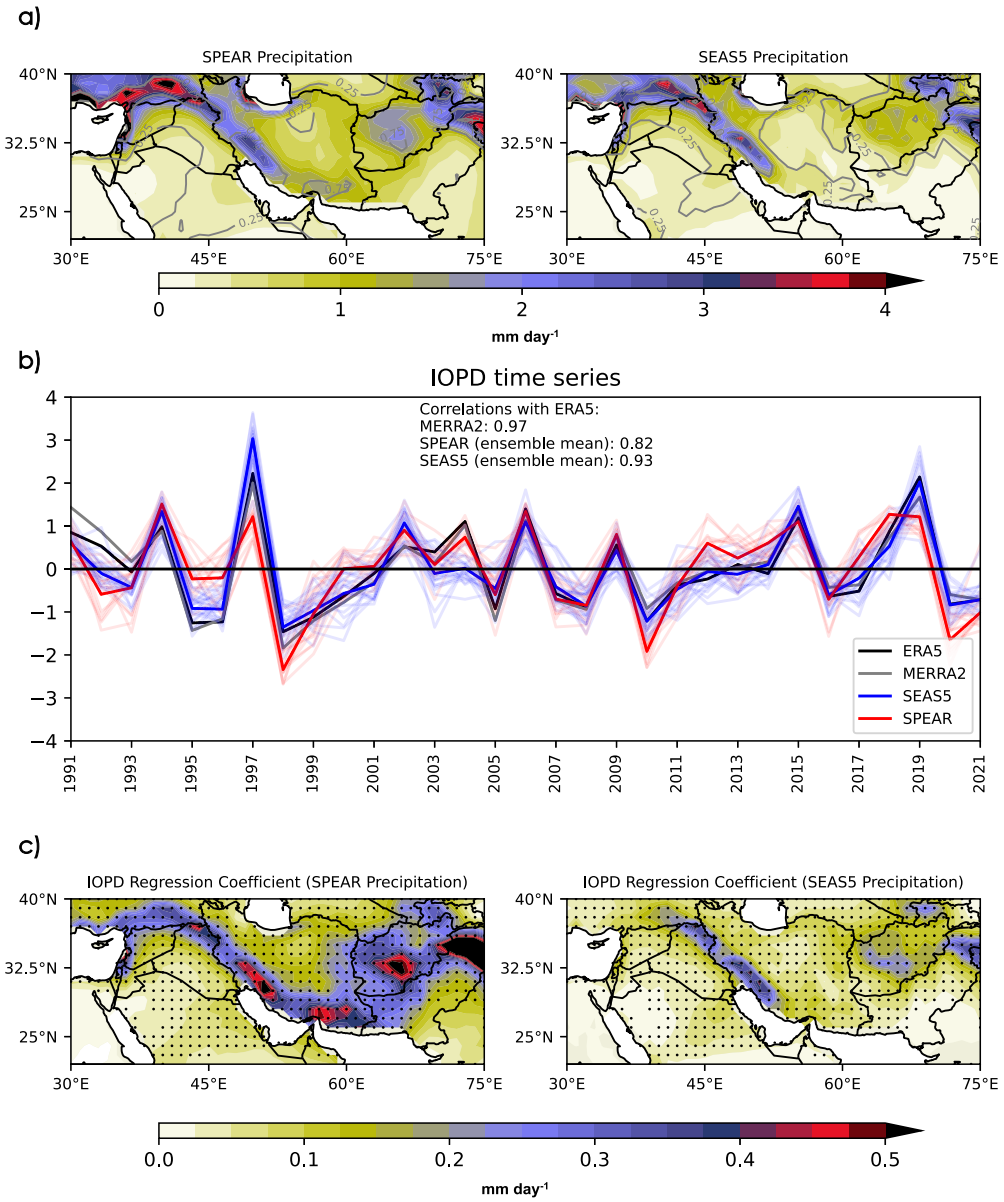

Fig. 5 | CSWA precipitation and tropical teleconnections in SEAS5 and SPEAR. **a** Average precipitation (color;mm day^{-1}) and standard deviation (contour; mm day^{-1}). Standard deviation is defined as the mean standard deviation of all model members. **b** Standardized IOPD index in SEAS5 (blue) and SPEAR (red), ERA5 (black), and MERRA2 (grey). Light colour lines represent individual ensemble members in SEAS5 and SPEAR. The correlation numbers are based on ERA5. **c** CSWA Precipitation (mm day^{-1}) onto the standardized IOPD index after concatenating ensemble members. Stippling indicates statistical significance at the 95% confidence level.

Interestingly, the addition of ENSO direct forcing as an independent variable in the regression model does not add much to the explained variance (<1%; Supplementary Fig. 11). The lack of significant influence of direct ENSO forcing in the presence of IOPD is consistent with our earlier findings that seasonal ENSO's influence over CSWA during winter is predominantly mediated by its indirect pathway through the Indian Ocean. While we use reanalyzed (ERA5 and MERRA2) precipitation as our primary reference datasets, interannual precipitation variability has also been shown based on CRU and CPC data. The spatially averaged reanalyzed precipitation data (ERA5 and MERRA2) correspond well with grid-based observations (CRU and CPC). The correlation coefficient exceeds 0.93 in all cases.

Our analysis establishes that combining identified tropical and extratropical forcings can explain three-fourths of area-averaged winter precipitation variability over the CSWA region. Therefore, representing these forcings in seasonal forecasting systems would be imperative for reliably predicting winter precipitation in this region. With this knowledge, we now analyze GFDL and ECMWF seasonal prediction systems to investigate their skillfulness over the CSWA region and its linkage to accuracy in representing identified tropical and extratropical forcings.

Tropical and extratropical forcings in SEAS5 and SPEAR

As a next step, we explore the representation of tropical and extratropical forcings in SEAS5[33] and SPEAR[32], and their relationship to seasonal predictability of winter precipitation over CSWA. The ensemble mean of precipitation in both modelling systems reasonably captures elevation-driven magnitude heterogeneity (Fig. 5a). However, winter precipitation over northern Pakistan, Tajikistan, Turkmenistan, Afghanistan, and eastern Iran is relatively lower in SEAS5 than SPEAR and two reanalyses. Furthermore, SEAS5 exhibits less interannual precipitation variability than SPEAR and reanalyses for most of these regions, while SPEAR exhibits substantially higher variability over Afghanistan and northwestern CSWA than reanalyses (Fig. 5a).

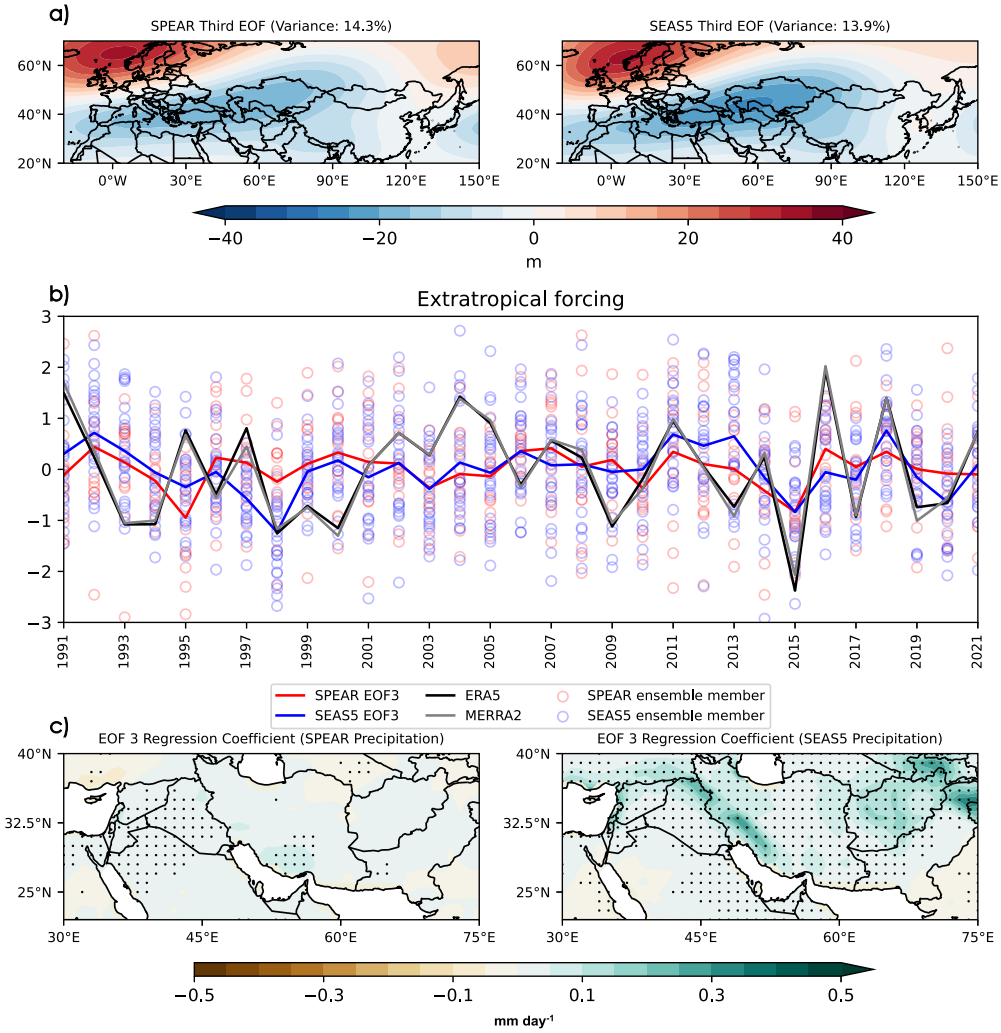

Fig. 6 | Extratropical forcing in SEAS5 and SPEAR. a The second EOF of 200 hPa geopotential height of concatenated model data after linearly removing ENSO and IOPD influences (**b**) Standardized EOF3 PC in SEAS5 (blue) and SPEAR (red), with EOF2 PC in ERA5 (black), and MERRA2 (grey). Light colour circles represent individual ensemble members in SEAS5 and SPEAR. The correlation numbers are based on ERA5 (**c**) Regression of CSWA precipitation (mm day^{-1}) onto EOF3 indices.

The two modelling systems represent the first mode of SST variability in the equatorial Pacific Ocean, precipitation variability in the tropical Indian Ocean (Fig. 5b), and IOPD and ENSO interannual variability exceptionally well (Fig. 5b, Supplementary Fig. 12). The correlation between reanalyses and models' ensemble mean ENSO indexes is 0.95 or greater (Supplementary Fig. 12). SEAS5 IOPD also exhibits an exceptionally high correlation with reanalyses-based IOPD indexes (ERA5: 0.93, MERRA2: 0.89). The SPEAR IOPD index correlation is also high with reanalyses but slightly weaker than SEAS5 (ERA5: 0.82, MERRA2: 0.80). Relatively lower correlations between the SEAS5/SPEAR ensemble mean and ERA5/MERRA2 reanalyses in the case of IOPD than ENSO are understandable as the IOPD index is based on precipitation whereas the ENSO index is based on SST. Precipitation anomalies, in general, are spatiotemporally more variable than SSTs, and therefore, it is more challenging to represent them in model simulation with very high accuracy.

The regression of CSWA precipitation anomalies onto the IOPD index based on the concatenated ensemble data in SEAS5 and SPEAR yields widespread positive influence consistent with reanalyses (Fig. 5c). However, the magnitude of the SPEAR regression coefficient is substantially higher than SEAS5, especially over mountainous regions in Pakistan, Afghanistan, and Iran. The higher magnitudes over the Zagros mountains in Iran and Iraq are comparable with those in reanalyses (Fig. 2c), while those in Afghanistan and northern Pakistan are stronger. Compared to the reanalyses, SPEAR exhibits higher precipitation variability, contributing to its stronger IOPD and CSWA precipitation relationship. Conversely, compared to the reanalyses, seasonal precipitation magnitude and variability are lower in SEAS5. As a result, the regression coefficient describing the IOPD and CSWA relationship in SEAS5 is less strong. These results are consistent if regression is performed on the ensemble mean rather than the concatenated ensemble data (Supplementary Fig. 13).

While tropical forcing is accurately reproduced in both seasonal modelling systems, extratropical forcing relevant to CSWA winter precipitation variability needs improvements in representation (Fig. 6, Supplementary Fig. 14). To highlight this point, EOF analyses are conducted for the concatenated ensemble of SEAS5 and SPEAR, using the same criteria as for reanalyses, i.e., both ENSO and IOPD influences are linearly removed from each ensemble member individually before concatenation and EOF analyses on 200-hPa geopotential height over a domain between 20°W–150°E longitudes and 20°N–70°N latitudes. The CSWA-relevant EOF pattern in models and reanalyses is similar, except that it is the second EOF in Fi in models (Fig. 6, Supplementary Fig. 14). The pattern correlation between ERA5 EOF2 and SEAS5 (SPEAR) EOF3 is 0.83 (0.85). The respective correlations are slightly higher at 0.85 (0.88) between models and MERRA2. However, the zonally elongated trough across CSWA is weaker in SPEAR's EOF3. Relatively lower pattern correlations are exhibited for other corresponding EOFs in ERA5 and models (Supplementary Fig. 14).

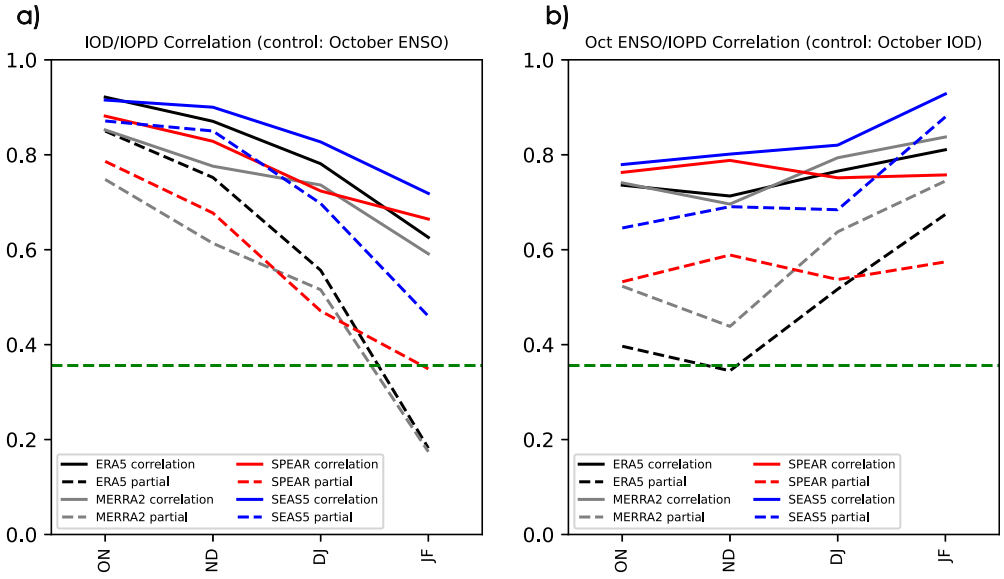

Fig. 7 | IOPD, IOD, and ENSO Correlation. a The correlation of the October IOD in ERA5 (black), MERRA2 (grey), SEAS5 (blue), and SPEAR (red) with overlapping two-month IOPD between October and March. Dashed lines represent partial correlations controlled for October ENSO values. **b** same as (**a**) but for ENSO values. Dashed lines represent partial correlations controlled for IOD values.

Unfortunately, while the model-based EOF3 has a strong spatial correspondence with the reanalyses-based EOF2, the seasonal prediction of the corresponding PCs (Fig. 6b) lacks substantial skill. The correlation skill in SEAS is marginally significant but low ($r = 0.35$), whereas the skill in SPEAR is statistically insignificant ($r = 0.19$). The correlation of SEAS5 PC3 with the CSWA precipitation index is also statistically significant (0.34) but weaker than the corresponding correlations in reanalyses (~0.5). SPEAR PC3 does not significantly correlate with the CSWA precipitation index. A regression of CSWA precipitation onto concatenated PC3 in SEAS5 shows a widespread statistically significant impact on CSWA precipitation variability. This is associated with strong regression coefficients in northern Pakistan, Tajikistan, Afghanistan, and the Zagros mountains in Iran. Though weaker, the SEAS5 regression pattern matches reasonably well with those in the reanalyses (Fig. 6c). SPEAR, on the other hand, mostly shows negligible influence. Together, these results highlight a lack of skill in representing extratropical forcing, particularly in SPEAR, which should limit winter precipitation predictability over the CSWA region in these seasonal forecasting systems.

The insignificant (SPEAR) or marginally significant (SEAS5) skill in predicting the CSWA-relevant atmospheric mode (Fig. 6) indicates either substantial biases in the seasonal prediction systems or that most of the seasonal variability of these modes can be attributed to seasonally unpredictable atmospheric noise. Previous studies suggest that the spatial structure of such extratropical modes can be robustly represented in model simulations, such as SEAS5 and SPEAR, but their seasonal evolution is often unpredictable on interannual timescales[41]. Dynamical models demonstrate some skill in the seasonal predictability of NAO, the leading mode of atmospheric variability in the northern hemisphere[31]. When relevant sources of predictability are identified, empirical models are even better at predicting seasonal NAO evolution[42]. The CSWA-relevant atmospheric mode, however, is closely related to less prevalent atmospheric modes in the northern hemisphere. Therefore, the seasonal predictability of such modes and determining their sources of predictability is more challenging.

However, there is evidence that IOPD-based tropical forcing can be predicted well in advance (Fig. 5b). Recent studies suggest that October IOD and contemporaneous ENSO can affect precipitation variability in the western Indian Ocean during early winter[43]. To understand this phenomenon more deeply, we analyze the association of bi-monthly IOPD with the October pre-conditioning of IOD and ENSO. In October, ENSO and IOD are strongly correlated (ERA5 = 0.67; MERRA2 = 0.62).

Consequently, we have conducted partial correlation analyses in addition to Pearson correlations to determine their combined and independent roles in IOPD variability (Fig. 7). As the season progresses, the correlation between IOD (ENSO) and IOPD decreases (increases) without controlling for ENSO (IOD). The October IOD correlation with winter IOPD declines sharply after we control for ENSO, from a very strong (ERA5 = 0.85; MERRA2 = 0.75) in October-November to insignificant in the late winter (<0.2; January-February; Fig. 7a). In contrast, after controlling for IOD, October ENSO correlation with winter IOPD sharply increases from ~0.4 in October-November to >0.6 in January-February (Fig. 7b). By analyzing the monthly EOF pattern that defines IOPD, we can explain the weakening correlation with October IOD and a strengthening correlation with October ENSO. As the winter progresses, precipitation in the western Indian Ocean weakens (Supplementary Fig. 15), which correlates more with IOD[43]. Hence, IOD loses its influence over IOPD. On the other hand, ENSO strongly correlates with IOPD and eastern IO precipitation. Due to this, it maintains its correlation strength. SEAS5 and SPEAR represent this fundamental characteristic of October IOD and ENSO pre-conditioning on IOPD though their associations are overly strong in SEAS5, whereas ENSO's association remains relatively unchanged in SPEAR.

Predictability of CSWA precipitation in SEAS5 and SPEAR

Based on prediction skill, potential predictability, and their ratio (see "Methods" section), we analyze CSWA winter precipitation predictability in models (Fig. 8, Supplementary Fig. 16). SPEAR has a much higher potential predictability than SEAS5 (Fig. 8a). There are only a few regions of SEAS5 that show statistically significant potential predictability, such as Afghanistan, parts of Tajikistan, Turkmenistan, and the Zagros mountains in Iran. SPEAR, on the other hand, exhibits significant potential predictability across all regions. There is a lower ratio (<1; red; Fig. 8c, Supplementary Fig. 16) of prediction skill to potential practicability in northern Pakistan, Tajikistan, the Arabian Peninsula, and northwestern Central Asia. In these regions, the ensembles of the models strongly agree with each other, indicating overconfidence. Both models show areas of under-confidence (ratio >1; blue) in parts of the northern Arabian Peninsula (Iraq, Syria) and Turkmenistan. Additionally, SEAS5 has low confidence in parts of Afghanistan and Iran. These results indicate that model-based potential predictability estimates in SEAS5 may not represent true predictability, suggesting that CSWA winter precipitation may be more predictable[44,45].

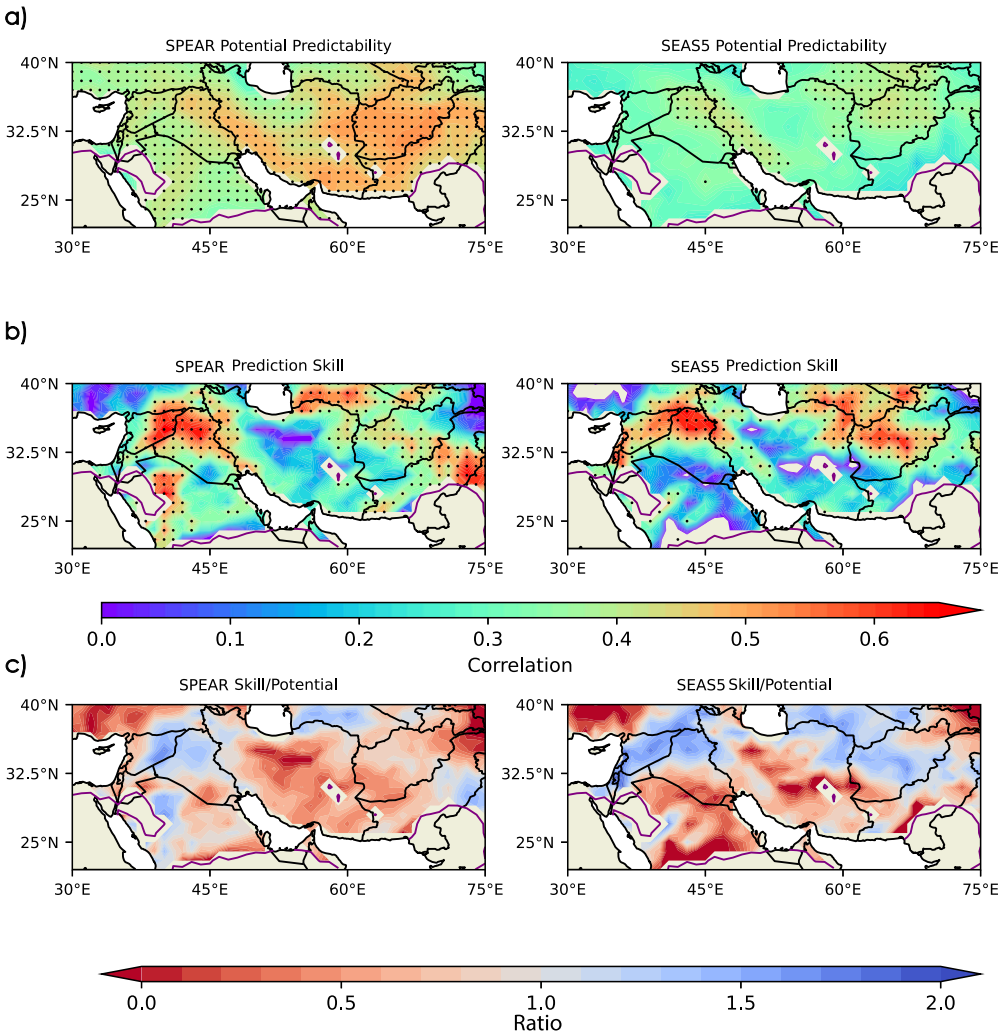

Fig. 8 | Predictability measures in SEAS5 and SPEAR. a Potential predictability in (left) SPEAR and (right) SEAS5. **b** Prediction skill calculated as anomaly correlation between the SEAS5 and SPEAR ensemble mean and ERA5. Stippling indicates statistical significance at the 95% confidence level. **c** The ratio of (**b** divided by **a**). In all panels, areas where the ERA5 mean precipitation is less than 0.2 mm day^{-1} are masked.

The interannual variability of CSWA winter precipitation in SEAS5, SPEAR, reanalysis (ERA5, MERRA2), regression model, and observations (CRU, CPC) is shown in Fig. 9a. This figure adds SPEAR and SEAS5 results, and their mean, to those already shown in Fig. 4 and Supplementary Fig. 7. Hollow circles represent individual ensemble members. Seasonal forecasting systems are less capable of capturing area-averaged interannual winter precipitation variability over CSWA than regression models. The low skill in the models can be explained based on the analyses presented so far in this study. The regression model considers the effects of tropical (ENSO) and extratropical (internal atmospheric variability) forcings on CSWA precipitation. Almost half of the variability in area-averaged CSWA winter precipitation can be attributed to IOPD (indirect ENSO) forcing. Extratropical influences explain a further 50% of the remaining half. Tropical forcing is quite accurately represented in SPEAR and SEAS5, but extratropical forcing is not. The atmospheric mode in the northern hemisphere (EOF2 in reanalyses) that influences CSWA precipitation variability is present in models but exhibits interannual variability inconsistent with that observed in reanalyses (Figs. 4a, 6c, Supplementary Fig. 9). Therefore, a lack of skill in simulating its correct interannual variability limits its potential role in improving the predictability of CSWA precipitation in models. In fact, it may be possible that misaligned interannual variability of extratropical forcing is responsible for reducing the ENSO-driven predictability of CSWA precipitation in these modelling systems.

It should be noted that SEAS5 performs slightly better in predicting CSWA precipitation in ERA5/MERRA2 ($R2 = 0.63/0.60$) than SPEAR ($R2 = 0.60/0.56$), owing to its relatively better representation of interannual variability of extratropical forcing. However, the unequal size of ensembles (SEAS = 25; SPEAR = 15) may affect correlations between ensemble mean and reanalysis. Therefore, to rule out this possibility, we examine the impact of ensemble size on correlations through bootstrapping in which 15 ensemble members of SEAS5 are randomly selected 1000 times (Fig. 9b), and the resultant ensemble mean is compared with results from reanalyses and observations. According to the histogram generated by this analysis, SEAS5 remains slightly superior to SPEAR. Hence, the ensemble size in the two modelling systems does not affect these results. Nonetheless, it is reasonable to assume that a large portion of CSWA winter precipitation is inherently less predictable in dynamical models since at least 25% of the variability comes from less prevalent internal atmospheric variability or atmospheric noise.

We have identified two key modes of natural variability that explain three-fourths of area-averaged winter precipitation variability in the CSWA region. The dominant teleconnection comes from the dipole of atmospheric diabatic heating anomalies in the Indian Ocean as an indirect ENSO influence. ENSO-induced changes in the Walker circulation cause opposite precipitation anomalies in the western and eastern Indian oceans. These anomalies constitute the first EOF pattern of precipitation variability in the tropical Indian Ocean and explain ~38% of the variance. Together, these

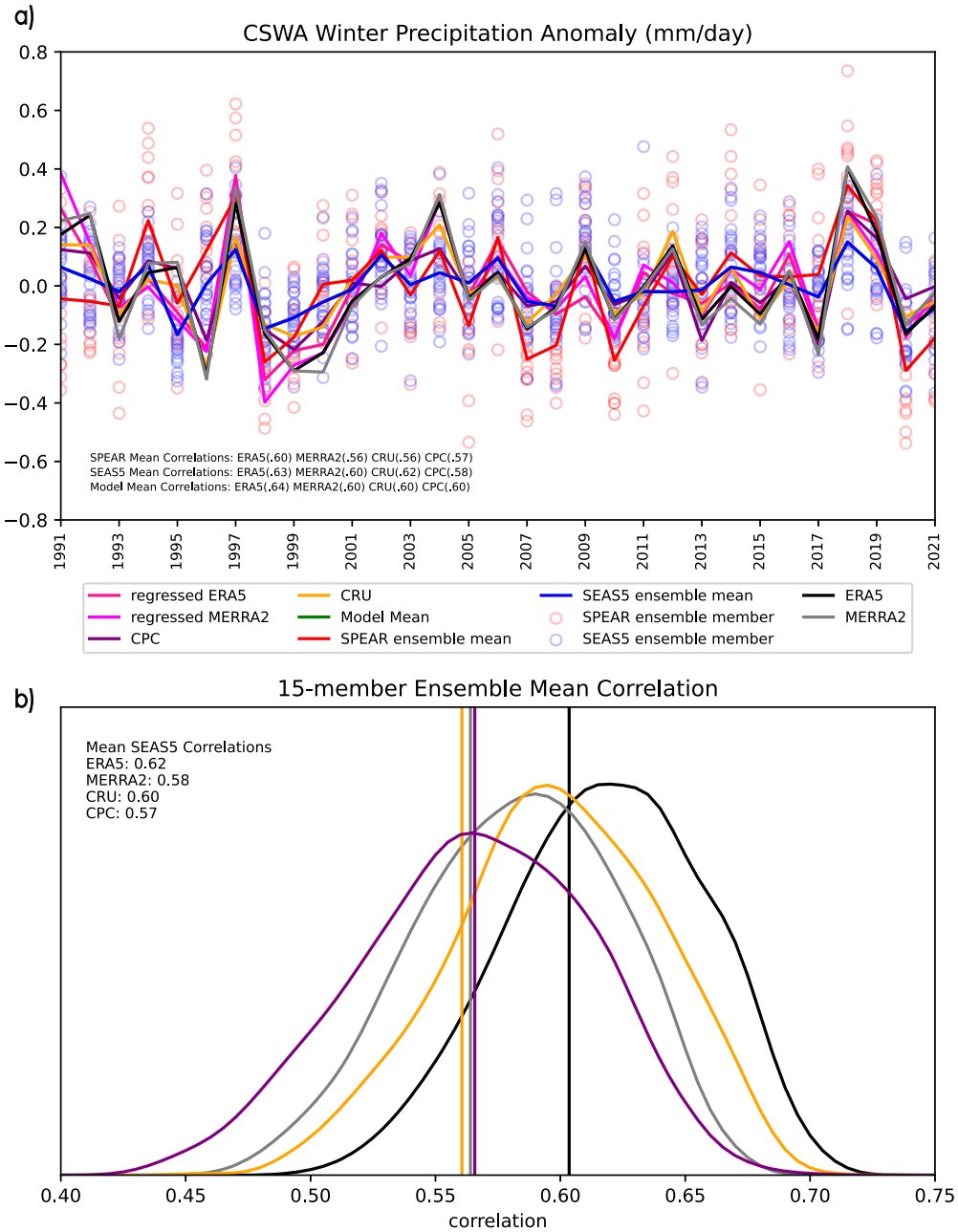

Fig. 9 | CSWA precipitation in SEAS5 and SPEAR. a Time series of area-average CSWA winter precipitation in reanalysis (ERA5, MERRA2), observations (CRU, CPC), reanalyses-based regression model, and models' ensemble mean (SEAS5, SPEAR, model mean). Each ensemble member in SEAS5 and SPEAR is shown as a hollow circle. Models' correlations with reanalyses and observations are shown. **b** Correlation histogram of 1000 instances of randomly chosen 15 of 25 ensemble members from SEAS5 with observations and reanalyses. Lines are made using a Gaussian KDE. Vertical lines indicate the correlation in SPEAR.

anomalies induce a Rossby wave response in higher latitudes, providing a mechanism to influence precipitation variability in extratropical regions[9,18,46]. Over the CSWA region, the teleconnection is widespread, significantly positive, and accounts for ~50% of the area-averaged precipitation variability in winter on a seasonal scale.

The second forcing influencing winter precipitation variability in the CSWA region is a large-scale climate mode primarily arising from internal atmospheric variability in the northern hemisphere. The CSWA-relevant atmospheric mode is depicted in the second EOF pattern of upper-atmosphere geopotential in ERA5 and MERRA2 reanalysis data over a broad region covering the East Atlantic to Central Pacific between 20°N and 70°N. At the seasonal scale, this pattern predominantly represents the negative phase of EAM but also resembles positive EAWR and POL/EUR patterns. It shows a trough zonally spanning through CSWA, facilitating the movement of extratropical systems in the region. This EOF mode in upper-atmosphere geopotential height fields persists after ENSO forcing removal and should be considered an independent mechanism related to internal atmospheric variability in the northern hemisphere. Its influence on area-averaged CSWA winter precipitation accounts for ~50% of the remaining unexplained variance.

ENSO-driven tropical forcing is well represented in seasonal forecasting systems, SEAS5 and SPEAR. The models not only produce the modes of SST variability in the equatorial Pacific (direct ENSO forcing) and precipitation variability in the Indian Ocean (indirect ENSO forcing) but also exhibit exceptional skill in representing their interannual variability. Both positively influence CSWA precipitation, consistent with reanalyses. On the other hand, CSWA-relevant extratropical forcing requires improvement. Its spatial pattern is represented reasonably well in both

modelling systems. However, while SEAS5 accurately represents its interannual variability and teleconnection over the CSWA region, SPEAR fails to do so. Given that the CSWA-relevant extratropical mode represents internal atmospheric variability or atmospheric noise, its year-to-year evolution at a seasonal scale may be inherently limited. Further investigation using other seasonal forecasting systems is necessary to understand these limitations related to the predictability of internal atmospheric variability.

Methods

Data

This study uses two reanalysis datasets: the ECMWF fifth-generation reanalysis (ERA5)[47] and NASA's Modern-Era Retrospective Analysis for Research and Applications Version 2 (MERRA2)[48]. The use of multiple datasets helps ensure the robustness of key findings. Each dataset provides sea surface temperature (SST), 200-hPa geopotential height, and precipitation variables. Moreover, we use precipitation observations from Climate Research Unit (CRU) version 4.07[49] and the Climate Prediction Center Global Unified Gauge-Based Analysis of Daily Precipitation (CPC)[50].

Hindcast data from two seasonal forecasting systems, the ECMWF fifth-generation seasonal forecast system (SEAS5)[33] and the GFDL's Seamless System for Prediction and Earth Systems Research (SPEAR)[32], are analyzed for their skillfulness over the CSWA region. We use data from one-month lead simulations, initialized in October each year, and evaluate the mean of SST, 200-hPa geopotential height, and precipitation for the winter months (November to February). SPEAR data includes a 15-member ensemble from 1991 to 2019 and a 30-member ensemble from 2020 onwards. However, for consistency, we use the first 15 members. Similarly, SEAS5 data includes a 25-member ensemble for the period before 2017 and a 51-member ensemble from 2017 onwards, but for consistency, we restrict our analyses to the first 25 members.

The analyses cover November through February from 1991 to 2022. This is the only period when all reanalyses, observations, and seasonal forecasting systems have overlapping data. Note that a mid-1980s shift in tropical forcing teleconnection over the CSWA region was reported in recent studies[15,51]. Therefore, using a period after the reported shift also ensures that conclusions are less sensitive to the choice of the analysis period. All datasets are remapped to $1° \times 1°$ grid spacing using bilinear interpolation. All analyses are carried out after removing the linear trend from each data and each ensemble member. Detrending removes large data trends, such as those driven by increasing global temperatures, that may obscure other factors contributing to precipitation variability and changing cyclical patterns.

Indexes

The CSWA region is defined as the land area between 22°N to 40°N and 30°E to 70°E. We apply a land/sea mask using the North American Space Administration's (NASA) integrated multi-satellite retrieval for the GPM dataset[52] and define land as any grid cell under 25% water. An area average over this region defines the CSWA precipitation index.

To define tropical and extratropical forcing that influence CSWA precipitation, we use Empirical Orthogonal Function (EOF) analysis. Tropical forcing includes indexes representing SST variability in the equatorial Pacific and precipitation variability in the tropical Indian Ocean. ENSO diversity impacts its teleconnection with remote regions. Therefore, instead of selecting one of the four Niño indexes, we define the ENSO index as the principal component (PC) of the first EOF of SSTs in the Pacific covering 160°E to 80°W and 10°S to 10°N. The first EOF explains 82.7% (MERRA2: 81.5%) of the SST variability in the selected area in the Pacific Ocean and closely relates to all four Niño indexes of ENSO (Fig. 1, Supplementary Fig. 2). Precipitation variability in the tropical Indian Ocean during winter is closely associated with ENSO variability in the Pacific Ocean. It exhibits a dipole pattern in the western and eastern Indian Oceans. In earlier studies[9,18], the Indian Ocean winter precipitation variability index was calculated using two rectangle boxes in the western and eastern Indian oceans[18]. In this study, we define this index as the PC of the first EOF of precipitation from 40°E to 140°E and 10°S to 10°N. The EOF-based index over a broad region avoids sensitivity to area choice for rectangle boxes. The EOF-based precipitation index closely relates to the index used in earlier studies[9,18] (Fig. 1c, Supplementary Fig. 1).

The extratropical forcing is identified by EOF analyses of 200-hPa geopotential height, covering 20°W to 150°E and 20°N to 70°N, after linearly removing tropical forcings (ENSO and IOPD) and correlating PCs to CSWA precipitation index to find the most relevant mode. We find that the second EOF (EOF2) represents the CSWA-relevant extratropical forcing in reanalyses, and therefore, its PC represents the extratropical forcing index.

The selected domain for EOF analyses generally covers the CSWA and surrounding regions, where atmospheric variability is expected to have the strongest influence on the CSWA precipitation distribution in winter. However, it is important to remember that domain choice may influence how the EOF analysis turns out. Therefore, in addition to our preferred choice of domain for EOF analyses, we also conduct these analyses using a domain that covers the entire Northern Hemisphere, a domain smaller than the selected region, and a domain larger than the selected region to test for sensitivity of the EOFs to the domain choice. A close resemblance is observed between the temporal variability of the PCs corresponding to EOF2 across all domains (Supplementary Fig. 17), indicating that the identified extratropical variability pattern is not sensitive to the domain choice.

There is also the possibility that only removing ENSO and IOPD cannot fully eliminate the tropical influence on atmospheric variability since these factors do not include variations in SSTs in the Atlantic and Indian Oceans, which may also influence atmospheric variability in the region of interest. We therefore investigate this issue following Hu et al.[53] (hereafter H22), which defines tropical forcing as the first six EOFs of tropical SSTs. Due to the weak coupling between IOPD and SSTs in the Indian Ocean in winter, we also remove IOPD from 200-hPa geopotential height after linearly removing tropical forcing defined by H22. The comparison of EOFs obtained after removing tropical forcing from the geopotential height using the original methodology (ENSO and IOPD), H22 alone, and H22 and IOPD combined suggests a negligible effect of Atlantic and Indian SST variability on the atmospheric modes of variability in this region (Supplementary Fig. 18). A correlation of 0.87 exists between the PCs of EOF2 in the original approach and the one following H22, which increases to 0.94 when the IOPD influence is removed after H22. EOF1 PC in revised approaches also compares strongly with the original method (0.88 and 0.86, respectively).

Based on the above findings, we only consider ENSO and IOPD influences when performing EOF analyses on simulated geopotential height data from SEAS5 and SPEAR. In the case of SEAS5 and SPEAR, EOF analyses are performed on the concatenated data, resulting in 465 (775) time steps in SPEAR (SEAS5). The CSWA-relevant extratropical forcing is represented by the third EOF (EOF3) in both models.

Analyses

We compare the EOF2 pattern in reanalyses with the northern hemisphere atmospheric modes defined by the Climate Prediction Center[36] (https://ftp.cpc.ncep.noaa.gov/wd52dg/data/indices/tele_index.nh). For this purpose, we regress 200-hPa geopotential height anomalies onto the CPC indexes after linearly removing tropical forcings from both, then calculate the correlation between EOF2 and the regressed patterns. Pattern correlation between reanalyses-based EOF2 and models-based EOFs identifies the comparable EOF pattern in SPEAR and SEAS5. To compare the interannual variability of extratropical mode between reanalyses and models, PC values corresponding to individual ensemble members are used to calculate the ensemble average for a given year.

We investigate the influences of tropical and extratropical forcings by performing linear and multiple linear regression of CSWA precipitation onto their indexes. For SPEAR and SEAS5 analyses, these regressions are performed using the ensemble mean and concatenated ensemble. All results are tested for significance at 95% confidence using a two-sided Student *t*-test. Additionally, the *F*-test determines the importance of each explanatory variable in the regression model.

We determine the potential predictability as the square root of the ratio of signal variance (the year-to-year variance of ensemble mean precipitation at any given point) divided by the sum of signal variance and noise variance (the variance of each ensemble member over the full timeframe of the model)[45,54]. This provides an estimate of the limit of predictability of the model based on the noise provided by the ensemble members. We define the prediction skill as the anomaly correlation between the ensemble mean of precipitation at any given point and our reanalysis data. A higher (lower) prediction skill than the potential predictability indicates an underconfident (overconfident) model[44,45].

SEAS5 and SPEAR have unequal ensemble sizes (25 and 15, respectively) that may influence their ensemble mean correlations with CSWA precipitation. We investigate this sensitivity by randomly selecting 15 members from SEAS5 and using their ensemble mean in correlation analyses. The process is repeated 1000 times and results are presented in a histogram smoothed with a Gaussian kernel.

Data availability

All datasets used in this analysis are publicly available. The ERA5 reanalysis and SEAS5 model data are available from the Copernicus Climate Change Service (C3S) Climate Date Store (https://cds.climate.copernicus.eu/). MERRA2 reanalysis data are available from NASA Data and Information Services System (https://disc.gsfc.nasa.gov/datasets?project=MERRA-2). SPEAR data is available from the North American Multi-model Ensemble archive (http://iridl.ldeo.columbia.edu/SOURCES/.Models/.NMME/.GFDL-SPEAR/). CPC Data is available from NOAA's Physical Sciences Laboratory (https://psl.noaa.gov/data/gridded/data.cpc.globalprecip.html). CRU Data is available from the climactic research unit (https://crudata.uea.ac.uk/cru/data/hrg/).

Code availability

All code is available upon request to the authors.

Received: 18 June 2023; Accepted: 15 February 2024;
Published online: 26 March 2024

References

1. Funk, C. et al. Recognizing the famine early warning systems network: over 30 years of drought early warning science advances and partnerships promoting global food security. *Bull. Am. Meteorol. Soc.* **100**, 1011–1027 (2019).
2. Barlow, M., Cullen, H. & Lyon, B. Drought in Central and Southwest Asia: La Niña, the Warm Pool, and Indian Ocean Precipitation. *J. Clim.* **15**, 697–700 (2002).
3. Barlow, M. et al. A review of drought in the Middle East and Southwest Asia. *J. Clim.* **29**, 8547–8574 (2016).
4. Syed, F. S., Adnan, S., Zamreeq, A. & Ghulam, A. Identification of droughts over Saudi Arabia and global teleconnections. *Nat. Hazards* **112**, 2717–2737 (2022).
5. Hoell, A. et al. The forcing of monthly precipitation variability over Southwest Asia during the Boreal Cold Season. *J. Clim.* **28**, 7038–7056 (2015).
6. Xie, T. et al. Mechanism of winter precipitation variations in the southern arid Central Asia. *Int. J. Climatol.* **42**, 4477–4490 (2022).
7. Syed, F. S., Giorgi, F., Pal, J. S. & King, M. P. Effect of remote forcings on the winter precipitation of central southwest Asia part 1: observations. *Theor. Appl. Climatol.* **86**, 147–160 (2006).
8. Horan, M. F. et al. Moisture sources for precipitation variability over the Arabian Peninsula. *Clim. Dyn.* **61**, 4793–4807 (2023).
9. Mehmood, S. et al. Dominant controls of cold-season precipitation variability over the high mountains of Asia. *NPJ Clim. Atmos. Sci.* **5**, 1–13 (2022).
10. Dimri, A. P. et al. Western disturbances: a review. *Rev. Geophys.* **53**, 225–246 (2015).
11. Kamil, S. et al. Long-term ENSO relationship to precipitation and storm frequency over western Himalaya–Karakoram–Hindukush region during the winter season. *Clim. Dyn.* **53**, 5265–5278 (2019).
12. Hunt, K. M. R., Turner, A. G. & Shaffrey, L. C. The evolution, seasonality and impacts of western disturbances. *Q. J. R. Meteorol. Soc.* **144**, 278–290 (2018).
13. Romanou, A. et al. Evaporation–precipitation variability over the Mediterranean and the Black Seas from satellite and reanalysis estimates. *J. Clim.* **23**, 5268–5287 (2010).
14. Syed, F. S., Giorgi, F., Pal, J. S. & Keay, K. Regional climate model simulation of winter climate over Central–Southwest Asia, with emphasis on NAO and ENSO effects. *Int. J. Climatol.* **30**, 220–235 (2010).
15. Rana, S., McGregor, J. & Renwick, J. Dominant modes of winter precipitation variability over Central Southwest Asia and inter-decadal change in the ENSO teleconnection. *Clim. Dyn.* **53**, 5689–5707 (2019).
16. Atif, R. M. et al. Extreme precipitation events over Saudi Arabia during the wet season and their associated teleconnections. *Atmos. Res.* **231**, 104655 (2020).
17. Mariotti, A., Ballabrera-Poy, J. & Zeng, N. Tropical influence on Euro-Asian autumn rainfall variability. *Clim. Dyn.* **24**, 511–521 (2005).
18. Abid, M. A., Ashfaq, M., Kucharski, F., Evans, K. J. & Almazroui, M. Tropical Indian Ocean Mediates ENSO influence over central southwest asia during the wet season. *Geophys. Res. Lett.* **47**, e2020GL089308 (2020).
19. Liu, H., Liu, X. & Dong, B. Intraseasonal variability of winter precipitation over central Asia and the western Tibetan plateau from 1979 to 2013 and its relationship with the North Atlantic Oscillation. *Dyn. Atmos. Oceans* **79**, 31–42 (2017).
20. Gerlitz, L. et al. Variability of the cold season climate in Central Asia. Part I: weather types and their tropical and extratropical drivers. *J. Clim.* **31**, 7185–7207 (2018).
21. Ehsan, M. A., Kucharski, F. & Almazroui, M. Potential predictability of boreal winter precipitation over central-southwest Asia in the North American multi-model ensemble. *Clim. Dyn.* **54**, 473–490 (2020).
22. Almazroui, M., Abid, M. A., Athar, H., Islam, M. N. & Ehsan, M. A. Interannual variability of rainfall over the Arabian Peninsula using the IPCC AR4 Global Climate Models. *Int. J. Climatol.* **33**, 2328–2340 (2013).
23. Ehsan, M. A. et al. Skill and predictability in multimodel ensemble forecasts for Northern Hemisphere regions with dominant winter precipitation. *Clim. Dyn.* **48**, 3309–3324 (2017).
24. Almazroui, M. et al. Skill assessment of Saudi-KAU and C3S models in prediction of spring season rainfall over the Arabian Peninsula. *Atmos. Res.* **280**, 106461 (2022).
25. Barlow, M., Hoell, A. & Agel, L. An evaluation of CMIP6 historical simulations of the cold season teleconnection between tropical Indo-Pacific Sea surface temperatures and precipitation in Southwest Asia, the Coastal Middle East, and Northern Pakistan and India. *J. Clim.* **34**, 6905–6926 (2021).
26. Tippett, M. K., Barlow, M. & Lyon, B. Statistical correction of central Southwest Asia winter precipitation simulations. *Int. J. Climatol.* **23**, 1421–1433 (2003).
27. Shirvani, A., Landman, W. A., Barlow, M. & Hoell, A. Evaluation of the forecast skill of North American Multi-Model Ensemble for monthly and seasonal precipitation forecasts over Iran. *Int. J. Climatol.* **43**, 1141–1166 (2023).
28. O'Reilly, C. H. et al. Projections of northern hemisphere extratropical climate underestimate internal variability and associated uncertainty. *Commun. Earth Environ.* **2**, 1–9 (2021).
29. Anderson, J. et al. Present-day capabilities of numerical and statistical models for atmospheric extratropical seasonal simulation and prediction. *Bull. Am. Meteorol. Soc.* **80**, 1349–1362 (1999).

30. Thornton, H. E., Smith, D. M., Scaife, A. A. & Dunstone, N. J. Seasonal predictability of the East Atlantic pattern in late autumn and early winter. *Geophys. Res. Lett.* **50**, e2022GL100712 (2023).
31. Scaife, A. A. et al. Skillful long-range prediction of European and North American winters. *Geophys. Res. Lett.* **41**, 2514–2519 (2014).
32. Delworth, T. L. et al. SPEAR: the next generation GFDL modeling system for seasonal to multidecadal prediction and projection. *J. Adv. Model. Earth Syst.* **12**, e2019MS001895 (2020).
33. Johnson, S. J. et al. SEAS5: the new ECMWF seasonal forecast system. *Geosci. Model Dev.* **12**, 1087–1117 (2019).
34. Hoell, A., Barlow, M. & Saini, R. The leading pattern of intraseasonal and interannual Indian Ocean precipitation variability and its relationship with Asian circulation during the Boreal Cold Season. *J. Clim.* **25**, 7509–7526 (2012).
35. Rana, S., Renwick, J., McGregor, J. & Singh, A. Seasonal prediction of winter precipitation anomalies over Central Southwest Asia: a canonical correlation analysis approach. *J. Clim.* **31**, 727–741 (2018).
36. Barnston, A. G. & Livezey, R. E. Classification, seasonality and persistence of low-frequency atmospheric circulation patterns. *Mon. Weather Rev.* **115**, 1083–1126 (1987).
37. Mezzina, B., García-Serrano, J., Bladé, I. & Kucharski, F. Dynamics of the ENSO teleconnection and NAO variability in the North Atlantic–European late winter. *J. Clim.* **33**, 907–923 (2020).
38. Zhang, W. et al. Impact of ENSO longitudinal position on teleconnections to the NAO. *Clim. Dyn.* **52**, 257–274 (2019).
39. Saeed, S., Kucharski, F. & Almazroui, M. Impacts of mid-latitude circulation on winter temperature variability in the Arabian Peninsula: the explicit role of NAO. *Clim. Dyn.* **60**, 147–164 (2023).
40. Donat, M. G. et al. Changes in extreme temperature and precipitation in the Arab region: longterm trends and variability related to ENSO and NAO. *Int. J. Climatol.* **34**, 581–592 (2014).
41. Lledó, L., Cionni, I., Torralba, V., Bretonnière, P.-A. & Samsó, M. Seasonal prediction of Euro-Atlantic teleconnections from multiple systems. *Environ. Res. Lett.* **15**, 074009 (2020).
42. Wang, L., Ting, M. & Kushner, P. J. A robust empirical seasonal prediction of winter NAO and surface climate. *Sci. Rep.* **7**, 279 (2017).
43. Abid, M. A., Kucharski, F., Molteni, F. & Almazroui, M. Predictability of Indian Ocean precipitation and its North Atlantic teleconnections during early winter. *NPJ Clim. Atmos. Sci.* **6**, 17 (2023).
44. Scaife, A. A. & Smith, D. A signal-to-noise paradox in climate science. *NPJ Clim. Atmos. Sci.* **1**, 1–8 (2018).
45. Eade, R. et al. Do seasonal-to-decadal climate predictions underestimate the predictability of the real world? *Geophys. Res. Lett.* **41**, 5620–5628 (2014).
46. Joshi, M. K., Abid, M. A. & Kucharski, F. The role of an Indian Ocean heating dipole in the ENSO teleconnection to the North Atlantic European region in early winter during the twentieth century in reanalysis and CMIP5 simulations. *J. Clim.* **34**, 1047–1060 (2021).
47. Hersbach, H. et al. The ERA5 global reanalysis. *Q. J. R. Meteorol. Soc.* **146**, 1999–2049 (2020).
48. Gelaro, R. et al. The modern-era retrospective analysis for research and applications, Version 2 (MERRA-2). *J. Clim.* **30**, 5419–5454 (2017).
49. Harris, I., Osborn, T. J., Jones, P. & Lister, D. Version 4 of the CRU TS monthly highresolution gridded multivariate climate dataset. *Sci. Data* **7**, 1–18 (2020).
50. Xie, P. et al. A gauge-based analysis of daily precipitation over East Asia. *J. Hydrometeorol.* **8**, 607–626 (2007).
51. Kang, I. S., Rashid, I. U., Kucharski, F., Almazroui, M. & Alkhalaf, A. K. Multidecadal changes in the relationship between ENSO and wet-season precipitation in the Arabian Peninsula. *J. Clim.* **28**, 4743–4752 (2015).
52. Huffman, G. et al. Integrated Multi-satellitE Retrievals for GPM (IMERG) Land-Sea Mask NetCDF, Accessed 22 February 2023, https://gpm.nasa.gov/data/directory/imerg-land-sea-mask-netcdf.
53. Hu, S., Zhou, T. & Wu, B. The physical processes dominating the impact of the summer North Atlantic oscillation on the Eastern Tibetan Plateau summer rainfall. *J. Clim.* **35**, 7677–7690 (2022).
54. Osman, M. & Vera, C. S. Climate predictability and prediction skill on seasonal time scales over South America from CHFP models. *Clim. Dyn.* **49**, 2365–2383 (2017).

Acknowledgements

This research used the Oak Ridge Leadership Computing Facility resources, a DOE Office of Science User Facility supported under Contract DE-AC05-00OR22725. This work is supported by the U.S. Air Force Numerical Weather Modeling Program and National Climate-Computing Research Center, located within the National Center for Computational Sciences at the ORNL and supported under a Strategic Partnership Project 2316T849-08 between DOE and NOAA.

Author contributions

M.F.H. and M.A. designed the study. M.F.H. performed the analyses. All authors were involved in the discussion of results. M.A. and M.F.H. wrote the manuscript draft and finalized it with feedback from all authors.

Competing interests

The authors declare no competing interests.

Additional information

Supplementary information The online version contains supplementary material available at https://doi.org/10.1038/s41612-024-00594-5.

Correspondence and requests for materials should be addressed to Matthew F. Horan.